MOLECULAR BIOLOGY

Structure and mechanism of the plant RNA polymerase V

Guohui Xie[1]†, Xuan Du[2]†, Hongmiao Hu[1]†‡, Sisi Li[2], Xiaofeng Cao[3], Steven E. Jacobsen[4,5], Jiamu Du[1]*

In addition to the conserved RNA polymerases I to III (Pols I to III) in eukaryotes, two atypical polymerases, Pols IV and V, specifically produce noncoding RNA in the RNA-directed DNA methylation pathway in plants. Here, we report on the structures of cauliflower Pol V in the free and elongation conformations. A conserved tyrosine residue of NRPE2 stacks with a double-stranded DNA branch of the transcription bubble to potentially attenuate elongation by inducing transcription stalling. The nontemplate DNA strand is captured by NRPE2 to enhance backtracking, thereby increasing 3′-5′ cleavage, which likely underpins Pol V's high fidelity. The structures also illuminate the mechanism of Pol V transcription stalling and enhanced backtracking, which may be important for Pol V's retention on chromatin to serve its function in tethering downstream factors for RNA-directed DNA methylation.

Transcription by DNA-dependent RNA polymerases (DdRPs) transmits genetic information from DNA to RNA. Whereas RNA polymerases I to III (Pols I to III) are conserved in most eukaryotes (*1*), plants have two additional polymerases, Pols IV and V, that are involved in the plant-specific RNA-directed DNA methylation (RdDM) pathway (*2*–*7*). In RdDM, Pol IV transcripts are used by RNA-DEPENDENT RNA POLYMERASE 2 (RDR2) to produce double-stranded RNAs (dsRNAs), which are subsequently processed by DICER-LIKE 3 (DCL3) into small interfering RNAs (siRNAs) that are loaded into ARGONAUTE 4 (AGO4) (*8*–*19*). In a second downstream step, Pol V produces long noncoding RNA transcripts that serve as a scaffold to bind the AGO4-siRNA complex, which then recruits the DNA methyltransferase DOMAINS REARRANGED METHYLASE 2 (DRM2) to mediate DNA methylation and gene silencing (*20*–*24*). Therefore, Pol V serves the dual role of both producing transcripts and tethering other factors to chromatin. Despite having evolved from Pol II, the Pol IV-V–clade DdRPs have substitutions in multiple subunits and critical residues that are adapted to their distinctive functions (*25*–*27*). Pols IV and V were both reported to require RNA primers and to show weaker in vitro transcription activity as compared with Pol II (*12*). Pol IV is also more error-prone than Pol II, whereas Pol V was reported to have higher fidelity (*28*). Although structural studies have been essential for understanding the mechanism of Pols (*13*, *29*–*34*), determining a structure for Pol V has remained a challenge.

Structure determination of cauliflower Pol V

To investigate the Pol V transcription mechanism, we obtained a monoclonal antibody against a C-terminal peptide of cauliflower (*Brassica oleracea* var. *botrytis*) NRPE1, a distinctive Pol V subunit. We used this antibody to purify Pol V from cauliflower inflorescence (Fig. 1A and fig. S1, A and B), a tissue enriched in dividing cells and DdRPs (*35*, *36*). All 12 subunits of Pol V were confirmed in the purified material by mass spectroscopy (MS) (fig. S1, B and C). Although *Arabidopsis* Pol V was shown to only transcribe the bipartite scaffold of a template DNA (DNA_T) plus an RNA primer (*12*), the purified *B. oleracea* Pol V (*Bo*Pol V) showed substantial transcription activity toward both a bipartite scaffold and a transcription bubble (fig. S1, D and E). We determined the cryo–electron microscopy (cryo-EM) structures of *Bo*Pol V in both apo and transcription bubble–containing elongation complex (EC) conformations at 3.57- and 2.73-Å resolution, respectively (Fig. 1, figs. S2 to S4, and tables S1 and S2). Overall, the two structures were similar with a superimposition root mean square deviation of 0.8 Å. Despite being detected by MS, the NRPE4 and NRPE7 subunits could not be traced in the density, whereas the other 10 subunits could be traced and modeled in both states. In Pol II, the RPB4-RPB7 subcomplex interacts with [illegible] clamp domain of RPB2 and the C terminus of RPB1 (*37*). These two regions showed weak density in our Pol V structure, which suggests loose binding and/or flexible conformations of NRPE4-7, potentially explaining why they were missing in our structure.

Overall structure of *Bo*Pol V

Both Pols IV and V evolved from Pol II (*38*). In *Arabidopsis*, Pol V has distinctive subunits NRPE1, NRPE5, and NRPE7, whereas NRPE(D)2 and NRPE(D)4 are shared by Pols V and IV but are different from those in Pol II. All other small subunits are shared by Pols II, IV, and V (*27*). The overall structure of Pol V adopts the classic Pol architecture and resembles other Pols, especially Pol IV (fig. S5) (*13*, *30*, *31*, *33*). Like Pol IV, Pol V lacks the binding surface for Pol II transcription factors, such as the initiation-related factor TFIIB and cleavage-related factor TFIIS (fig. S6, A and B) (*39*, *40*). This is consistent with the lack of these factors in our MS data and indicates that Pol V acts via a distinctive regulatory mechanism compared with Pol II. Despite being encoded by different genes, NRPE5 resembles RPB5 of Pol II and NRPD5 of Pol IV (fig. S6C). By contrast, NRPE9, which is common to Pols II, IV, and V, displays notable structural differences in the different Pols. Although the NRPE9 N-terminal jaw domains of Pols II, IV, and V occupy similar positions, the C-terminal zinc ribbon domain of NRPE9 occupies a specific position to interact with NRPE1, which is different from that seen in Pol II, in which RPB9 interacts with RPB2 (fig. S6D) (*13*, *30*). Compared with Pol IV, the Pol V NRPE9 zinc ribbon domain resides in a similar position but has a ~40° rotation (fig. S6E) (*13*). The funnel domain of Pol V NRPE1 is ~50 residues shorter than that of Pol IV NRPD1, resulting in a reduced binding interface between NRPE1 and the NRPE9 zinc ribbon domain (figs. S6F and S7).

In the EC structure, the last 3′-end RNA nucleotide is linked to the RNA (fig. S4Q). It pairs with the DNA_T and occupies the +1 position (Fig. 2A), representing a pretranslocation conformation (*41*). In the active center of DdRPs, two Mg^{2+} ions, metals A and B, are involved in RNA substrate and incoming nucleoside triphosphate (NTP) binding and catalysis (fig. S8A) (*41*). Because we did not observe NTP binding in our structure, only one Mg^{2+} ion at the metal A binding site was observed to be coordinated by Asp^{449}, Asp^{451}, and Asp^{453} of NRPE1, forming the catalytic site, consistent with a previous biochemical and genetic study (*25*) (Fig. 2A and fig. S8B). Like other Pols, the active center of Pol V has two essential structural elements: the bridge helix (BH) and the trigger loop (TL) (Fig. 2A). The Pol V BH resembles the Pol II BH, despite multiple sequence variations (*29*, *41*) (Fig. 2B and fig. S7).

[1]Key Laboratory of Molecular Design for Plant Cell Factory of Guangdong Higher Education Institutes, Institute of Plant and Food Science, Department of Biology, School of Life Sciences, Southern University of Science and Technology, Shenzhen 518055, China. [2]Department of Biochemistry and Molecular Biology, International Cancer Center, Shenzhen University Medical School, Shenzhen 518060, China. [3]State Key Laboratory of Plant Genomics and National Center for Plant Gene Research, Institute of Genetics and Developmental Biology, Chinese Academy of Sciences, Beijing 100101, China. [4]Department of Molecular, Cell and Developmental Biology, University of California at Los Angeles, Los Angeles, CA 90095, USA. [5]Howard Hughes Medical Institute, University of California at Los Angeles, Los Angeles, CA 90095, USA.
*Corresponding author. Email: dujm@sustech.edu.cn
†These authors contributed equally to this work.
‡Present address: MRC Laboratory of Molecular Biology, Cambridge CB2 0QH, UK.

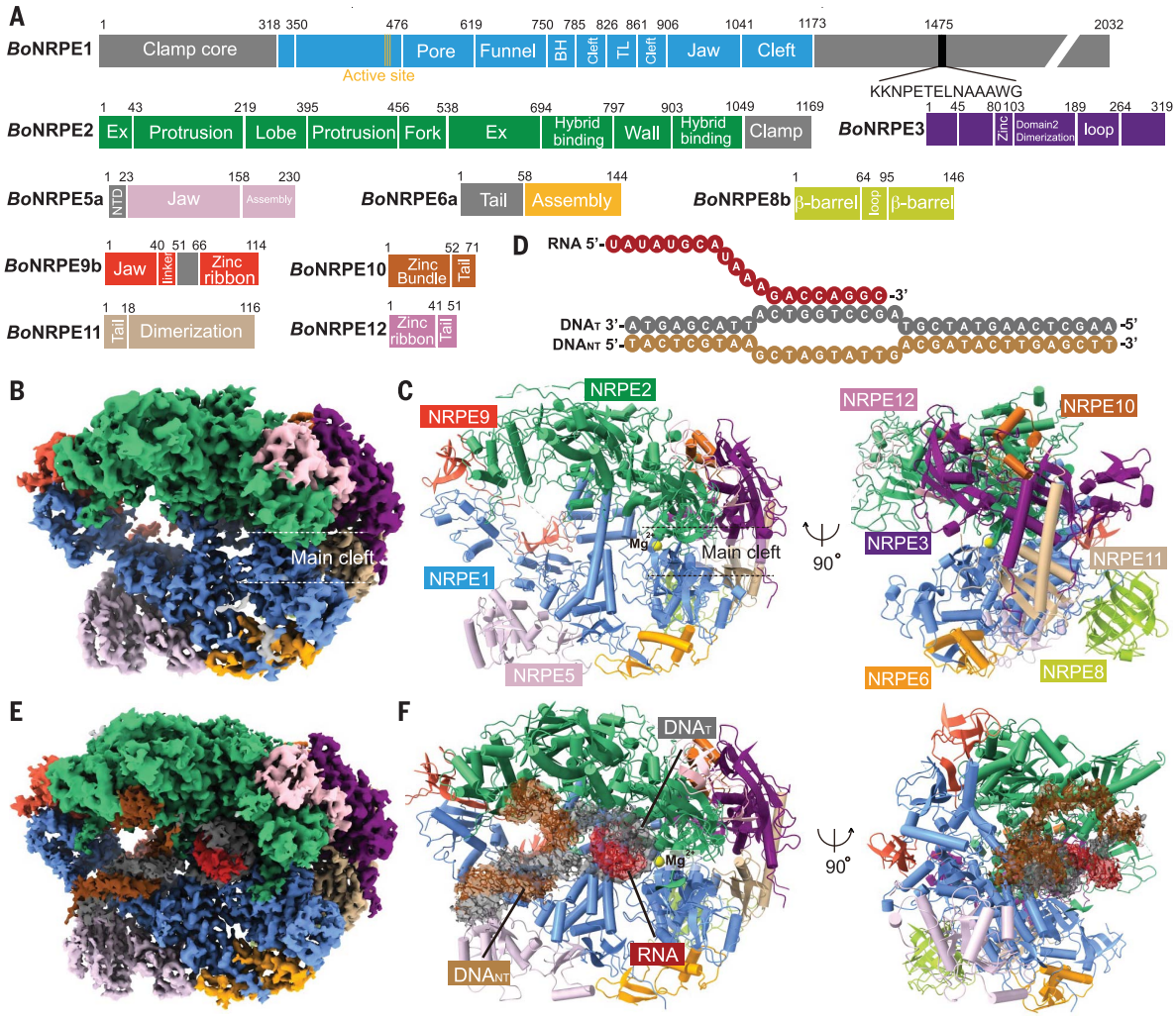

Fig. 1. Structures of *Bo*Pol V in apo and elongation conformations. (**A**) Domain architecture of *Bo*Pol V subunits. The sequence of NRPE1 C-terminal peptide for antibody production is listed. (**B**) Cryo-EM map of *Bo*Pol V in apo form. (**C**) Structure of *Bo*Pol V in the apo form. The subunits are colored as in (A). (**D**) Nucleic acid scaffold for EC formation. (**E**) Cryo-EM map of *Bo*Pol V in complex with a transcription bubble. (**F**) Structure of *Bo*Pol V in the elongation conformation.

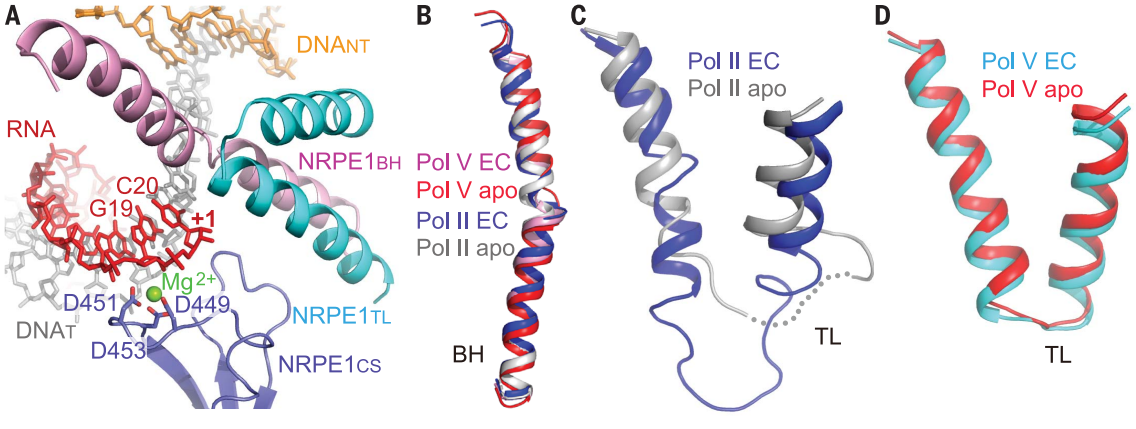

Fig. 2. Active-site conformation. (**A**) Active site of *Bo*Pol V. $NRPE1_{CS}$, catalytic site of NRPE1; $NRPE1_{BH}$, the bridge helix of NRPE1; $NRPE1_{TL}$, the trigger loop of NRPE1. (**B**) Superimposition of the BH of *Bo*Pol V in the apo and elongation states and yeast Pol II in the apo [Protein Data Bank (PDB) ID 1I50] and elongation (PDB ID 2E2H) states, which shows no appreciable conformational change. (**C** and **D**) Superimposition of the TL of yeast Pol II in the apo (PDB ID 1I50) and elongation (PDB ID 2E2H) states (C) and *Bo*Pol V in the apo and elongation states (D), which show that the TL of Pol II is more flexible, whereas Pol V TL is less flexible. D, Asp.

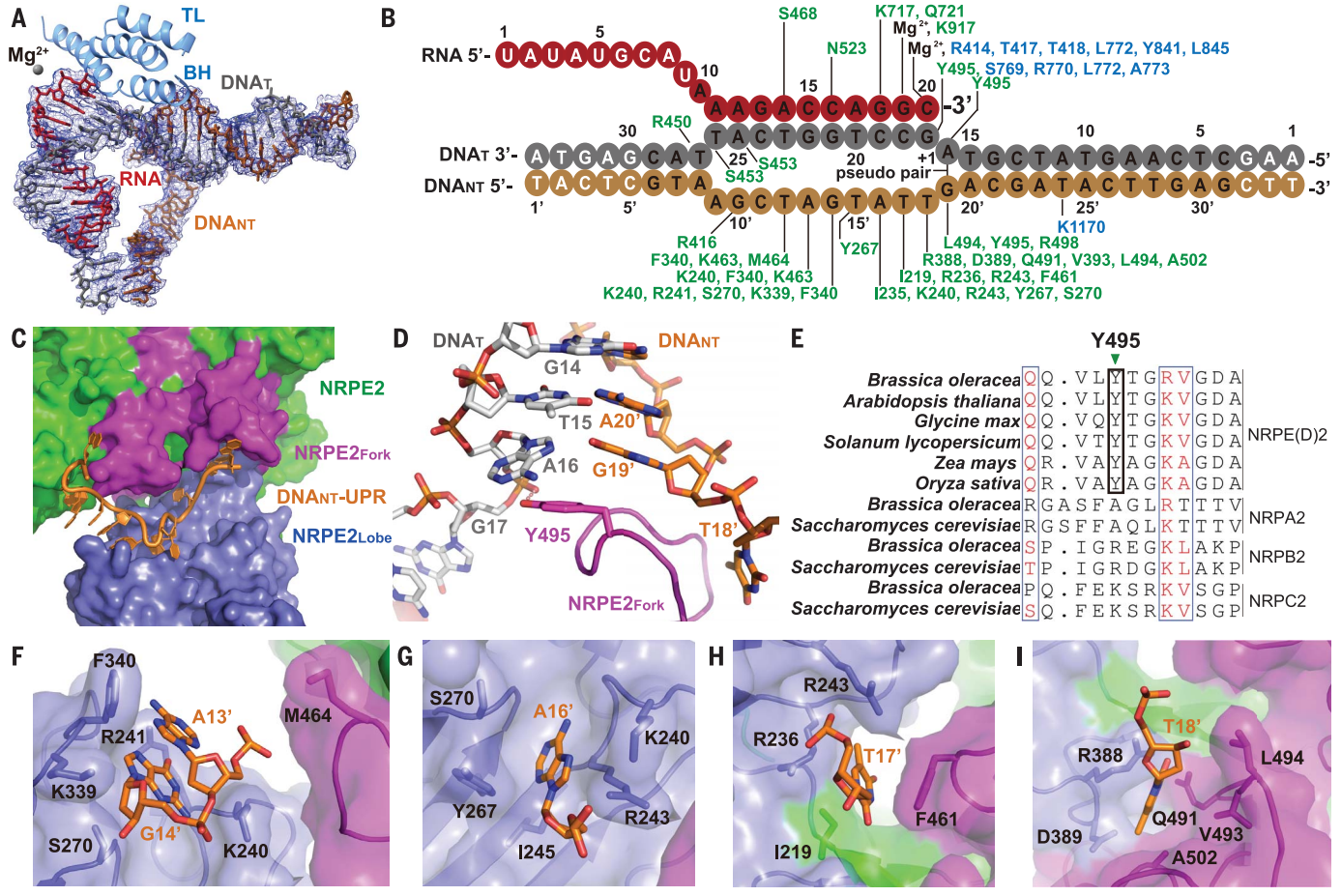

Fig. 3. The interaction between NRPE2 and the transcription bubble. (**A**) Cryo-EM map of the transcription bubble. (**B**) Schematic of the overall interactions between *Bo*Pol V and the transcription bubble. The nucleotides observed in the structure are colored in black and the unobserved ones in white. The residues of NRPE1 and NRPE2 are colored in blue and green, respectively. (**C**) DNA_{NT}-UPR is clamped between the NRPE2 fork ($NRPE2_{Fork}$) and lobe ($NRPE2_{Lobe}$) domains. Other regions of NRPE2 are colored in green. (**D**) $NRPE2_{Fork}$ residue Tyr^{495} stacks with the A16-G19′ pseudo-pair and hydrogen bonds with the phosphate group of G17. (**E**) Structure-based sequence alignment of the NRPE(D)2 from multiple species and NRPA2, NRPB2, and NRPC2 reveals that the Tyr^{495} is conserved only in the NRPE(D)2 clade but not in others. (**F** to **I**) DNA_{NT}-UPR bases G14′ (F), A16′ (G), T17′ (H), and T18′ (I) are accommodated by surface pockets of NRPE2. Single-letter abbreviations for the amino acid residues are as follows: A, Ala; C, Cys; D, Asp; E, Glu; F, Phe; G, Gly; H, His; I, Ile; K, Lys; L, Leu; M, Met; N, Asn; P, Pro; Q, Gln; R, Arg; S, Ser; T, Thr; V, Val; W, Trp; and Y, Tyr.

The Pol V TL is shorter than that in Pol II and also exhibits sequence variations (fig. S7). In contrast to the Pol II TL which shows conformational change in the transition from the apo form to the EC form (*29*, *41*) (Fig. 2C), the TL in both the Pol V apo and EC structures adopts a similar compacted conformation (Fig. 2D), which suggests less conformational flexibility of the Pol V TL. Compared with Pols I and III, although their BHs adopt conformations similar to that of Pol V (fig. S8, C and D), the TLs of Pols I and III are flexible such that they are partially disordered in both the apo and EC forms (fig. S8, E and F) (*31*, *33*, *42*). Given that the TL conformational dynamics is required for NTP substrate binding to promote the transcription reaction, the less-flexible Pol V TL may decrease the NTP incorporation, resulting in lower activity (*12*, *41*).

Interactions between NRPE2 and the transcription bubble

Except for some terminal nucleotides, the entire transcription bubble, including the unpaired region of the nontemplate DNA (DNA_{NT}-UPR), which is often disordered in Pol II structures (*43*, *44*), can be fully traced and modeled in our Pol V EC structure (Fig. 3, A and B). This is likely due to the extensive interactions between DNA_{NT}-UPR and NRPE2 (Fig. 3B), the shared second subunit of Pols IV and V. Overall, DNA_{NT}-UPR is clamped between the lobe and fork domains of NRPE2 (Fig. 3C). At the downstream double-stranded DNA (dsDNA) branching site of the transcription bubble, the first unpaired nucleotides, G19′ of the DNA_{NT} and A16 of the DNA_T, form a pseudo-pair (Fig. 3D), probably mimicking the last DNA base pair in natural transcription. The NRPE2 fork loop residue Tyr^{495}—which is conserved in NRPE(D)2 across multiple species, but not in the NRPA2, NRPB2, and NRPC2 clades (Fig. 3E)—specifically inserts to the DNA branching position to stack with the upcoming A16-G19′ pseudo-pair while also forming a hydrogen bond with the phosphate group of the DNA_T G17 (Fig. 3D). The specific stacking and hydrogen-bonding interactions by the bulky side chain of Tyr^{495} may help Pol V to stabilize the transcription bubble, potentially allowing Pol V pausing to help it serve as a scaffold to recruit downstream effectors, and not only to produce and release RNA transcripts. Moreover, bases G14′, A16′, T17′, and T18′ of DNA_{NT}-UPR are anchored, through extensive interactions, by a series of surface base-binding pockets on NRPE2 (Fig. 3, B and F to I), which stabilizes their relative positions and potentially slows down transcription. The Pol V–bound DNA_{NT}-UPR could be nicely modeled onto that of Pol IV but showed

the steric clashes with Pol I and III and a loss of specific interactions upon modeling into Pol II (fig. S9) (*13*, *30*, *31*, *33*), suggesting that this is a feature specific to the Pol IV-V clade.

*Bo*Pol V attenuates transcription elongation

To investigate the biochemical relevance of our structures, we performed in vitro transcription assays using purified *Bo*Pol V and transcription bubble substrates with different gaps between the RNA primer 3′ end and the downstream dsDNA branching site, which are stacked by Tyr^{495} in our structure (Fig. 4A, scaffolds 2 to 5). Pol V showed substantial transcription activity, with an accumulation of transcript corresponding to the unpaired region of DNA_T (DNA_T-UPR) (Fig. 4B). By contrast, the bipartite substrate lacking the DNA_{NT} did not show accumulation of a specific transcript (Fig. 4B), which demonstrates transcription pausing at the downstream DNA branching site, consistent with NRPE2 Tyr^{495} obstructing Pol V translocation at this site. Low levels of longer transcripts were also observed with the transcription bubble substrates (Fig. 4B), which indicates that Pol V has a weak ability to open downstream paired DNA. By contrast, purified cauliflower Pol II (fig. S10) produced longer transcripts without an accumulation of DNA_T-UPR transcription product (Fig. 4C), suggesting that transcription pausing at the branch site is a specific feature of Pol V, or more generally of the Pol IV-V clade, consistent with Tyr^{495} being conserved in NRPE(D)2 but not in that of the other clades (Fig. 3E). Our results suggest that Pol V has relatively high transcriptional activity on the DNA_T-UPR but is less efficient in opening paired DNA, likely because of the conserved bulky Tyr^{495} stacking with, and blocking access to, downstream paired DNA. Because the natural template is always fully paired, Pol V may constitutively exhibit low transcription activity, plausibly contributing to transcriptional pausing and thereby enhancing Pol V retention on chromatin to support its function in tethering chromatin factors to promote RdDM.

NRPE2–DNA_{NT}-UPR interactions enhance backtracking

Transcription pausing is a key step in the induction of transcription backtracking and subsequent 3′-5′ cleavage for proofreading (*39*, *45*). Consistent with transcription pausing, abundant bands corresponding to the RNA-backtracked 3′-5′ cleavage product were observed in our Pol V activity assays (Fig. 4 and fig. S1, D and E). In the presence of Mg^{2+} and absence of NTP, Pol V almost exclusively showed RNA primer cleavage activity without transcription elongation (Fig. 4C). EDTA inhibited this cleavage, which confirmed a Mg^{2+}-dependent cleavage mechanism, similar to that of Pol II (Fig. 4C) (*39*). Addition of NTP and Mg^{2+} triggered *Bo*Pol V transcription elongation while maintaining strong cleavage (Fig. 4C). By contrast, under the same reaction conditions, *Bo*Pol II showed stronger transcription elongation and lower cleavage activity (*12*, *28*) (Fig. 4C). For the DdRP proofreading function to achieve high fidelity (*45*), 3′-5′ cleavage is required, which is consistent with the hypothesis that enhanced 3′-5′ cleavage activity underpins the higher fidelity of Pol V (*28*).

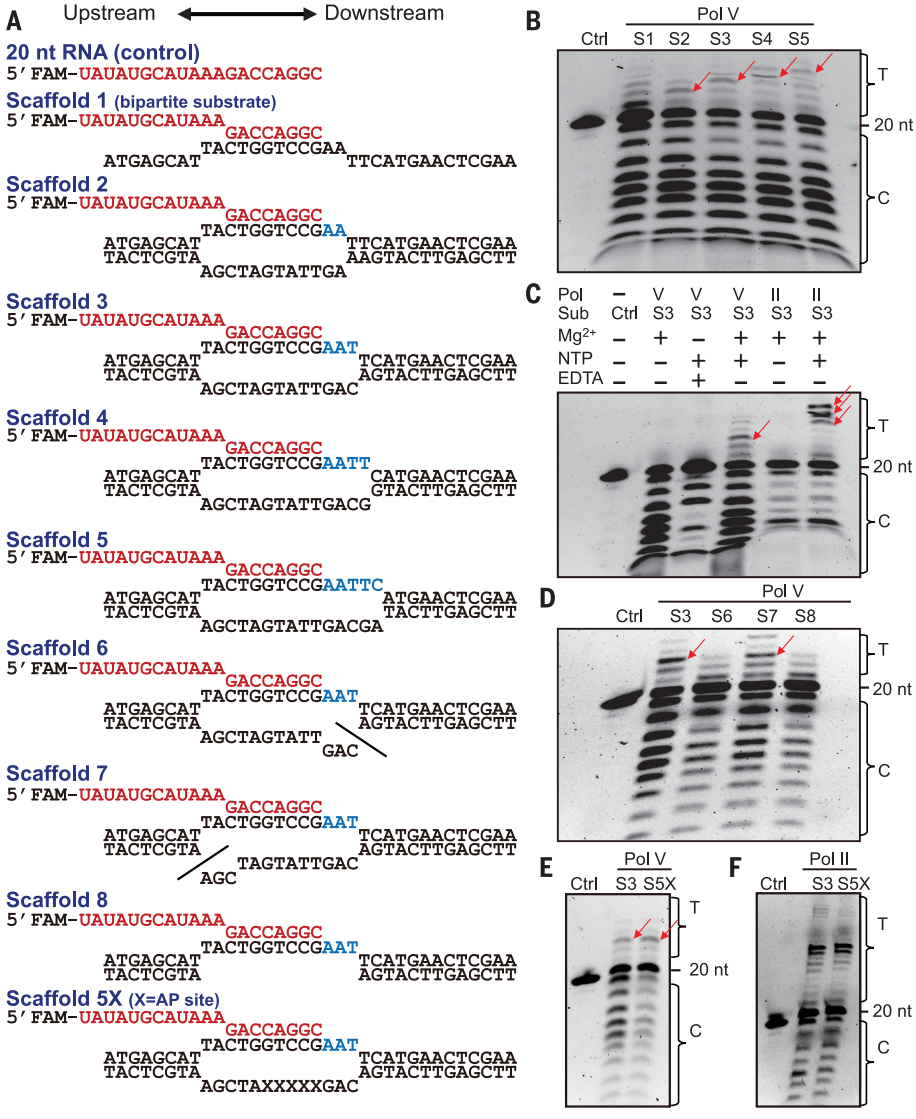

Fig. 4. In vitro biochemical assay. (**A**) Nucleic acid scaffold design. The RNA is 5′-labeled by fluorescein amidite (FAM) and highlighted in red, whereas the downstream DNA_T-UPR is highlighted in blue. In scaffolds 6 and 7, the oligos are disconnected at the lines. (**B**) Transcription assay using different substrate bubbles shows accumulation of transcription products of the downstream DNA_T-UPR, as highlighted by the red arrows. C, cleavage product; Ctrl, control; S1, scaffold 1; T, transcription product. (**C**) RNA primer 3′-5′ cleavage activity of Pol V is stimulated by Mg^{2+} and suppressed by EDTA, whereas transcription elongation requires NTP. Compared with Pol II, Pol V showed stronger 3′-5′ cleavage activity but weaker transcription activity. Sub, substrates. (**D**) Transcription assay using bubbles with different designs of the DNA_{NT} shows that the downstream DNA branching site and the DNA_{NT}-UPR are important for both the transcription and cleavage activities of Pol V. (**E** and **F**) Substitution of the NRPE2-interacting DNA_{NT}-UPR bases by AP sites reduced the 3′-5′ cleavage activity of Pol V (E) but not of Pol II (F), and these substitutions did not change transcription activity. The images shown in (B) to (F) are polyacrylamide gel electrophoresis (PAGE) results.

Excluding the A16-G19′ pseudo-pair, the Pol V transcription bubble contains a DNA_{NT}-UPR of 10 nucleotides (nt) with the downstream branching site–proximal bases T18′, T17′, A16′, and G14′ specifically captured by NRPE2 (Fig. 3, B and F to I), a Pol V–specific feature not observed in other Pols. To analyze the roles of the DNA_{NT}-UPR and the downstream branch in Pol V transcription, we designed a series of transcription bubbles. Compared with the

intact transcription bubble, breaking the DNA_{NT} at the downstream branch site or removing the DNA_{NT}-UPR (Fig. 4A, scaffolds 6 and 8) resulted in similar patterns that decreased both transcription and cleavage activities (Fig. 4D). This is likely because of the loss of interaction with the downstream reaction center in both cases. DNA_{NT} breakage at the upstream branch site (Fig. 4A, scaffold 7) resulted in almost full transcription activity and partial cleavage activity, relative to the intact bubble (Fig. 4D). Moreover, the shortening of DNA_{NT} while only keeping the downstream paired region decreased both the elongation and cleavage activities as well (fig. S11). Overall, these data suggest that the downstream branch and DNA_{NT}-UPR conformation both influence transcription and cleavage activity.

To investigate the NRPE2–DNA_{NT}-UPR interaction that is specific to Pol V (Fig. 3, B and F to I), we eliminated individual DNA_{NT}-UPR nucleotides by replacing them with an apurinic-apyrimidinic (AP) site while retaining DNA_{NT}-UPR integrity (fig. S12A). The loss of DNA_{NT}-UPR bases mildly reduced cleavage activity, with downstream bases having a greater effect than upstream ones (fig. S12B), which is consistent with downstream DNA_{NT}-UPR nucleotides having more interactions with NRPE2 (Fig. 3B). By contrast, all substitutions retained transcription activity similar to that of the unmodified substrate (fig. S12B). Nevertheless, all of the different individual substitutions only weakly affected cleavage activity. We also simultaneously substituted five contiguous downstream DNA_{NT}-UPR nucleotides with AP sites (Fig. 4A, scaffold 5X), which yielded a loss of cleavage activity but did not affect the elongation (Fig. 4E). By contrast, this multiple substitution showed no effect on either transcription or cleavage using *Bo*Pol II (Fig. 4F), which suggests that the importance of these base interactions is specific to Pol V, or likely the Pol IV-V clade. These results suggest that the interaction of the DNA_{NT}-UPR with NRPE2 is mainly responsible for enhancing Pol V cleavage activity. The 3′-5′ cleavage of all Pols requires transcription bubble backtracking to feed RNA into the active site on the largest subunit, that is, NRPE1 in Pol V. Therefore, the NRPE2–DNA_{NT}-UPR interaction promotes increased backtracking to feed RNA into NRPE1, resulting in enhanced Pol V 3′-5′ cleavage activity, a mechanism different from the intrinsic backtracking that is common in Pols.

Discussion

Distinct from Pols I to III, whose principal function is producing transcripts for release, Pols IV and V have evolved specialized transcription features adapted for RdDM. For example, Pol IV generates a single-stranded RNA 3′ end as a substrate for RDR2 through backtracking (*13*), and Pol V likely limits its transcription rate to prolong its chromatin occupancy, thereby providing a scaffolding function for the recruitment of chromatin factors. We speculate that the Pol IV-V–clade DdRPs evolved the shared NRPE(D)2 subunit so that they can stall transcription through the conserved NRPE(D)2 tyrosine residue and enhance backtracking through the NRPE(D)2–DNA_{NT}-UPR interactions. In the case of Pol V, the strong backtracking and transcription stalling may regulate the equilibrium between forward and backward steps, which delays termination and release of transcripts and thus leads to Pol V–long noncoding RNA complex retention on chromatin to promote its scaffolding function. This may also explain the short and relatively uniform length of Pol IV transcripts (35 to 50 nt) (*8*, *13*, *17*). Pol IV likely backtracks to feed RNA into RDR2 through an interpolymerase channel that likely bypasses cleavage (*13*), which may also explain its lower fidelity (*28*). Given NRPE(D)2-induced transcription stalling and high backtracking activity, Pol IV–RNA is unable to undergo long extension before backtracking. Pol IV–RNA may be captured by RDR2 once the nascent transcript is long enough to trigger the dsRNA synthesis by RDR2 and subsequent termination of Pol IV transcription (*13*).

REFERENCES AND NOTES

1. R. G. Roeder, W. J. Rutter, *Nature* **224**, 234–237 (1969).
2. J. R. Haag, C. S. Pikaard, *Nat. Rev. Mol. Cell Biol.* **12**, 483–492 (2011).
3. A. J. Herr, M. B. Jensen, T. Dalmay, D. C. Baulcombe, *Science* **308**, 118–120 (2005).
4. T. Kanno *et al*., *Nat. Genet.* **37**, 761–765 (2005).
5. M. A. Matzke, R. A. Mosher, *Nat. Rev. Genet.* **15**, 394–408 (2014).
6. Y. Onodera *et al*., *Cell* **120**, 613–622 (2005).
7. D. Pontier *et al*., *Genes Dev.* **19**, 2030–2040 (2005).
8. T. Blevins *et al*., *eLife* **4**, e09591 (2015).
9. X. Du *et al*., *Plant Cell* **34**, 2140–2149 (2022).
10. A. Fukudome *et al*., *Proc. Natl. Acad. Sci. U.S.A.* **118**, e2115899118 (2021).
11. V. Gasciolli, A. C. Mallory, D. P. Bartel, H. Vaucheret, *Curr. Biol.* **15**, 1494–1500 (2005).
12. J. R. Haag *et al*., *Mol. Cell* **48**, 811–818 (2012).
13. K. Huang *et al*., *Science* **374**, 1579–1586 (2021).
14. J. Singh, V. Mishra, F. Wang, H. Y. Huang, C. S. Pikaard, *Mol. Cell* **75**, 576–589.e5 (2019).
15. Q. Wang *et al*., *Science* **374**, 1152–1157 (2021).
16. Z. Xie, E. Allen, A. Wilken, J. C. Carrington, *Proc. Natl. Acad. Sci. U.S.A.* **102**, 12984–12989 (2005).
17. J. Zhai *et al*., *Cell* **163**, 445–455 (2015).
18. D. Zilberman, X. Cao, S. E. Jacobsen, *Science* **299**, 716–719 (2003).
19. D. Zilberman *et al*., *Curr. Biol.* **14**, 1214–1220 (2004).
20. X. Cao, S. E. Jacobsen, *Curr. Biol.* **12**, 1138–1144 (2002).
21. X. Cao, S. E. Jacobsen, *Proc. Natl. Acad. Sci. U.S.A.* **99**, 16491–16498 (2002).
22. G. Moissiard *et al*., *Science* **336**, 1448–1451 (2012).
23. A. T. Wierzbicki, T. S. Ream, J. R. Haag, C. S. Pikaard, *Nat. Genet.* **41**, 630–634 (2009).
24. X. Zhong *et al*., *Cell* **157**, 1050–1060 (2014).
25. J. R. Haag, O. Pontes, C. S. Pikaard, *PLOS ONE* **4**, e4110 (2009).
26. R. Landick, *Structure* **17**, 323–325 (2009).
27. T. S. Ream *et al*., *Mol. Cell* **33**, 192–203 (2009).
28. M. Marasco, W. Li, M. Lynch, C. S. Pikaard, *Nucleic Acids Res.* **45**, 11315–11326 (2017).
29. P. Cramer *et al*., *Science* **288**, 640–649 (2000).
30. P. Cramer, D. A. Bushnell, R. D. Kornberg, *Science* **292**, 1863–1876 (2001).
31. N. A. Hoffmann *et al*., *Nature* **528**, 231–236 (2015).
32. C. Engel, S. Sainsbury, A. C. Cheung, D. Kostrewa, P. Cramer, *Nature* **502**, 650–655 (2013).
33. C. Fernández-Tornero *et al*., *Nature* **502**, 644–649 (2013).
34. M. Girbig, A. D. Misiaszek, C. W. Müller, *Nat. Rev. Mol. Cell Biol.* **23**, 603–622 (2022).
35. T. J. Guilfoyle, *Biochemistry* **19**, 5966–5972 (1980).
36. L. Huang *et al*., *Nat. Struct. Mol. Biol.* **16**, 91–93 (2009).
37. K. J. Armache, S. Mitterweger, A. Meinhart, P. Cramer, *J. Biol. Chem.* **280**, 7131–7134 (2005).
38. S. L. Tucker, J. Reece, T. S. Ream, C. S. Pikaard, *Cold Spring Harb. Symp. Quant. Biol.* **75**, 285–297 (2010).
39. A. C. Cheung, P. Cramer, *Nature* **471**, 249–253 (2011).
40. S. Sainsbury, J. Niesser, P. Cramer, *Nature* **493**, 437–440 (2013).
41. D. Wang, D. A. Bushnell, K. D. Westover, C. D. Kaplan, R. D. Kornberg, *Cell* **127**, 941–954 (2006).
42. S. Neyer *et al*., *Nature* **540**, 607–610 (2016).
43. C. Bernecky, F. Herzog, W. Baumeister, J. M. Plitzko, P. Cramer, *Nature* **529**, 551–554 (2016).
44. H. Kettenberger, K. J. Armache, P. Cramer, *Mol. Cell* **16**, 955–965 (2004).
45. E. Nudler, *Cell* **149**, 1438–1445 (2012).

ACKNOWLEDGMENTS

We thank P. Wang, J. Tan, S. Xu, and X. Ma at the Southern University of Science and Technology (SUSTech) Cryo-EM Center for data collection; the SUSTech Core Research Facilities for help with MS experiments; and G. Riddihough (Life Science Editors) for editing. **Funding:** This work was funded by the Shenzhen Science and Technology Program (grants JCYJ20200109110403829 and KQTD20190929173906742 to J.D.); the Key Laboratory of Molecular Design for Plant Cell Factory of Guangdong Higher Education Institutes (grant 2019KSYS006 to J.D.); the China Postdoctoral Science Foundation (grant 2022M712173 to X.D.); the National Natural Science Foundation of China (grant 31788103 to X.C.); the Chinese Academy of Sciences Strategic Priority Research Program (grant XDB27030201 to X.C.); and the National Institutes of Health (grant R35 GM130272 S.E.J.). S.E.J. is an investigator of the Howard Hughes Medical Institute. **Author contributions:** Conceptualization: G.X., H.H., and J.D.; Methodology: G.X., X.D., H.H., S.L., and X.C.; Investigation: G.X., X.D., and H.H.; Funding acquisition: X.D., X.C., S.E.J., and J.D.; Project administration: J.D.; Supervision: X.C., S.E.J., and J.D.; Writing – original draft: J.D.; Writing – review and editing: S.E.J. and J.D. **Competing interests:** The authors declare no competing interests. **Data and materials availability:** The structures have been deposited in the Protein Data Bank under accession codes 8HIL and 8HIM. The cryo-EM maps have been deposited in the Electron Microscopy Data Bank under accession codes EMD-34820 and EMD-34821. The biological material is available upon request to J.D. All data are available in the main text or the supplementary materials. This research was funded in whole or in part by the Howard Hughes Medical Institute, a cOAlition S organization. The author will make the Author Accepted Manuscript (AAM) version available under a CC BY public copyright license.

SUPPLEMENTARY MATERIALS

science.org/doi/10.1126/science.adf8231
Materials and Methods
Figs. S1 to S12
Tables S1 and S2
References (*46*–*58*)
MDAR Reproducibility Checklist

View/request a protocol for this paper from *Bio-protocol*.

Submitted 5 December 2022; accepted 25 February 2023
Published online 9 March 2023
10.1126/science.adf8231

Structure and mechanism of the plant RNA polymerase V

Guohui Xie, Xuan Du, Hongmiao Hu, Sisi Li, Xiaofeng Cao, Steven E. Jacobsen, and Jiamu Du

Science, **379** (6638), .
DOI: 10.1126/science.adf8231

Chromatin retention of Pol V

A plant atypical RNA polymerase, Pol V, specifically synthesizes the scaffold long noncoding RNA for recruiting downstream effectors to chromatin to mediate DNA methylation. Xie *et al*. report the structure of a cauliflower Pol V in elongation conformation. Distinct from Pol II, the second subunit of Pol V, NRPE2, specifically stacks with the upcoming double-stranded DNA branch to attenuate transcription and captures the nontemplate DNA strand of the transcription bubble to enhance the backtracking, suggesting a chromatin retention mechanism underlying the scaffold function of Pol V. —DJ